Target inner-shells contributions to the stopping power and straggling for H and He ions in gold

Santiago Heredia-Avalos[1,4]**, Isabel Abril**[2]**, Cristian D Denton**[2]**, Juan Carlos Moreno-Marín**[3] **and Rafael Garcia-Molina**[1]

[1] Departamento de Física–CIOyN, Universidad de Murcia, Apartado 4021, E-30080 Murcia, Spain
[2] Departament de Física Aplicada, Universitat d'Alacant, Apartat 99, E-03080 Alacant, Spain
[3] Departament de Física, Enginyeria de Sistemes i Teoria del Senyal, Universitat d'Alacant, Apartat 99, E-03080 Alacant, Spain

E-mail: sheredia@um.es

Abstract
The electronic energy loss of swift H and He ions in gold is studied, paying special attention to the contribution to the projectile energy loss due to the ionization of the target inner-shells. We calculate the stopping power and the energy-loss straggling as a function of the projectile energy, taking into account the different charge states that the projectile can acquire inside the target and using the dielectric formalism. The electronic response of gold is described by the MELF-GOS model, where the excitation of valence and N-shell electrons is characterized by a linear combination of Mermin-type energy-loss functions, whereas the contribution to the projectile energy loss due to the target K-, L-, and M-shell ionization is included through hydrogenic generalized oscillator strengths.

Stopping powers and straggling are, respectively, systematically above and below the data in our linear response formulation when H and He ions are below 0.1 MeV/u. Our calculations show that the total contribution of K-, L-, and M-shells to stopping power and straggling is less than 0.5% and 3.5% below 1 MeV/u, respectively. For stopping powers, the contribution of these inner-shells increases to 9% at 10 MeV/u and continues to rise to 20% at 100 MeV/u. For straggling, it increases to 23% at 10 MeV/u and rises to 35% at 100 MeV/u.

(Some figures in this article are in colour only in the electronic version)

A precise knowledge of the stopping power and the energy-loss straggling of swift projectiles in matter is important for many practical applications in different research areas such as microelectronics, surface analysis, nuclear physics, space exploration, protection against radiation, and radio-therapeutic medicine [1–6].

[4] Author to whom any correspondence should be addressed.

There is a lot of experimental data in the literature about the inelastic energy loss of swift projectiles in solids for different projectile–target combinations [7], and several models have been developed to explain and predict these experimental results [8–12]. The behavior of several materials, such as gold and other transition metals with a broad excitation spectrum, cannot be treated as a free electron gas and requires a more realistic description [12].

In this work we use the dielectric formalism to calculate the stopping power and the energy-loss straggling of gold for swift H and He ions in order to analyze the influence of inner-shell excitations in the energy-loss processes. In this formalism the target is characterized through its energy-loss function (ELF) using the MELF-GOS model [12], where outer-shell electronic excitations are described by means of a linear combination of Mermin-type ELFs, whereas inner-shell electronic excitations are accounted for through hydrogenic generalized oscillator strengths (GOS). On the other hand, we use hydrogenic orbitals to describe the projectile electronic density, considering the different charge states the projectile can acquire, its polarization due to the self-induced electric field, and the energy loss due to electronic capture and loss processes.

When a swift atomic projectile (with atomic number Z_1) penetrates a material with velocity v, it begins to lose and capture electrons until charge equilibrium is reached after an elapsed time, which depends on the projectile–target combination as well as on the velocity of the former [13]. The stopping power S_p of the material is calculated as the weighted sum of the partial stopping powers $S_{p,q}$ for the different charge states q that the projectile can acquire during its travel through the target,

$$S_p = \sum_{q=0}^{Z_1} \phi_q \, S_{p,q}, \tag{1}$$

where ϕ_q is the probability of finding the projectile in a given charge state q, evaluated from the CasP 3.1 code [14]. In the energy range we are concerned with ($E \gtrsim 10$ keV/u), nuclear stopping power can be neglected, so $S_{p,q}$ can be obtained as [12]

$$S_{p,q} = \frac{2e^2}{\pi v^2} \int_0^\infty \frac{dk}{k} \left[Z_1 - \rho_q(k) \right]^2 \int_0^{kv} d\omega \, \omega \, \text{Im}\left[\frac{-1}{\epsilon(k,\omega)} \right]$$
$$+ \frac{2e^2 Z_1}{\pi v^2} \int_0^\infty \frac{dk}{k} \rho_q(k) \int_0^{kv} d\omega \, \omega \, \text{Im}\left[\frac{-1}{\epsilon(k,\omega)} \right] \left[1 - \cos\left(\frac{\omega d_q}{v} \right) \right], \tag{2}$$

where e is the absolute value of the electron charge, $\rho_q(k)$ is the Fourier transform of the projectile electronic density for the q charge state, $\hbar k$ and $\hbar \omega$ are, respectively, the momentum and energy transferred to electronic excitations of the target, $\hbar$ is Planck's constant, and $\text{Im}[-1/\epsilon(k,\omega)]$ is the target ELF.

Analogously, the energy-loss straggling Ω^2, defined as the variance in the energy-loss distribution per unit path length, can be written as a weighted sum over all possible charge states,

$$\Omega^2 = \sum_{q=0}^{Z_1} \phi_q \, \Omega_q^2, \tag{3}$$

where the partial contributions Ω_q^2 can be expressed in the dielectric formalism as [12]

$$\Omega_q^2 = \frac{2e^2 \hbar}{\pi v^2} \int_0^\infty \frac{dk}{k} \left[Z_1 - \rho_q(k) \right]^2 \int_0^{kv} d\omega \, \omega^2 \, \text{Im}\left[\frac{-1}{\epsilon(k,\omega)} \right]$$
$$+ \frac{2e^2 \hbar Z_1}{\pi v^2} \int_0^\infty \frac{dk}{k} \rho_q(k) \int_0^{kv} d\omega \, \omega^2 \, \text{Im}\left[\frac{-1}{\epsilon(k,\omega)} \right] \left[1 - \cos\left(\frac{\omega d_q}{v} \right) \right]. \tag{4}$$

The second term in equations (2) and (4) represents the contribution due to the polarization of the projectile caused by the self-induced electric field, which displaces by a distance $d_q = \alpha_q \, \mathcal{E}_q(v)$ the center of the projectile electronic cloud from its nucleus [12, 15]; α_q is the projectile polarizability [15] and $\mathcal{E}_q(v)$ is the self-induced electric field produced by the projectile,

$$\mathcal{E}_q = \frac{2e}{\pi v^2} \int_0^\infty \frac{\mathrm{d}k}{k} \left[Z_1 - \rho_q(k) \right] \int_0^{kv} \mathrm{d}\omega \, \omega \, \mathrm{Im} \left[\frac{-1}{\epsilon(k, \omega)} \right]. \tag{5}$$

We use hydrogenic wavefunctions to obtain $\rho_q(k)$,

$$\rho_q(k) = N \left[1 + \left(\frac{k}{2Z_1'} \right)^2 \right]^{-2}, \tag{6}$$

where N is the number of projectile bound electrons; $Z_1' = Z_1$ for hydrogenic projectiles (i.e. H^0 and He^+) and it must be replaced by the effective nuclear charge $Z_1' = Z_1 - 0.3$ for He^0, as stated by Slater's rules [16]. The additional screening by the target electrons is included by means of a Yukawa potential as proposed in [15].

In the MELF-GOS model we incorporate separately the contribution to the ELF due to outer-shell and inner-shell electrons [12], $\mathrm{Im}\,[-1/\epsilon(k, \omega)]_{\mathrm{outer}}$ and $\mathrm{Im}\,[-1/\epsilon(k, \omega)]_{\mathrm{inner}}$, respectively. Then

$$\mathrm{Im} \left[\frac{-1}{\epsilon(k, \omega)} \right] = \mathrm{Im} \left[\frac{-1}{\epsilon(k, \omega)} \right]_{\mathrm{outer}} + \mathrm{Im} \left[\frac{-1}{\epsilon(k, \omega)} \right]_{\mathrm{inner}}. \tag{7}$$

The ELF of gold associated to the weakly bound outer-shell electrons (valence and N-shell electrons) is obtained fitting the experimental ELF, in the optical limit ($k = 0$), by a linear combination of Mermin-type ELFs [8, 12]

$$\mathrm{Im} \left[\frac{-1}{\epsilon(k = 0, \omega)} \right]_{\mathrm{outer}} = \sum_i A_i \, \mathrm{Im} \left[\frac{-1}{\epsilon_{\mathrm{M}} \, (\omega_i, \gamma_i; \, k = 0, \omega)} \right], \tag{8}$$

where ϵ_{M} is the Mermin dielectric function [17]. In the above expression ω_i and γ_i are related to the position and width, respectively, of the ith Mermin-type ELF, whose corresponding weight is given by the coefficient A_i. This method warrants that the ELF is properly extended to $k \neq 0$ through the properties of the Mermin-type dielectric functions [18].

On the other hand, K-, L-, and M-shell electrons of gold have a marked atomic character and do not display collective effects; so their contribution to the ELF is modeled by means of atomic GOSs [19]

$$\mathrm{Im} \left[\frac{-1}{\epsilon(k, \omega)} \right]_{\mathrm{inner}} = \frac{2\pi^2 \mathcal{N}}{\omega} \sum_{n\ell} \frac{\mathrm{d} f_{n\ell}(k, \omega)}{\mathrm{d}\omega}, \tag{9}$$

where $\mathcal{N}$ is the atomic density of gold and $\mathrm{d} f_{n\ell}(k, \omega)/\mathrm{d}\omega$ is the GOS of the (n, ℓ) subshell. For the latter we use hydrogenic wavefunctions, because that description provides analytical expressions for the non-relativistic hydrogenic GOSs [12] and, in addition, these GOSs are practically identical to those evaluated by numerical methods [20].

It is worth mentioning that the ELF of gold associated with the N-shell electrons is modeled using Mermin-type ELFs [17] instead of GOSs [19] because these electrons are affected by the presence of neighboring atoms in the condensed system and display collective effects (see figure 1).

The parameters used to fit the ELF of gold were chosen in such a manner that it reproduces the main trends of the experimental ELF and satisfies the f-sum rule, i.e. the effective number
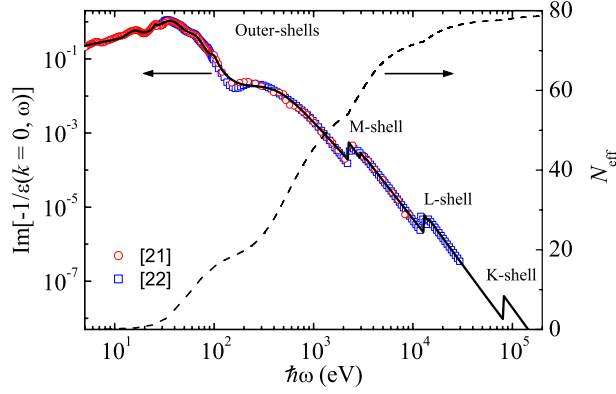
Figure 1. ELF of gold in the optical limit ($k = 0$) as a function of the excitation energy $\hbar\omega$. The solid curve corresponds to our model, whereas the symbols represent the experimental results from optical experiments [21] and from x-ray scattering factors [22]. The dashed curve represents N_{eff} as a function of the excitation energy $\hbar\omega$, see equation (10).

Table 1. Parameters used to fit, through equation (8), the ELF of Au, whose atomic density is $\mathcal{N} = 5.901 \, \text{Å}^{-3}$.

i	$\hbar\omega_i$ (eV)	γ_i (eV)	A_i
1	9.52	14.97	2.04×10^{-1}
2	15.92	6.26	1.02×10^{-1}
3	25.58	2.18	1.7×10^{-2}
4	38.09	26.67	6.71×10^{-1}
5	64.49	30.48	1.22×10^{-1}
6	99.32	19.05	9.01×10^{-3}
7	402.71	612.23	2.08×10^{-2}

of target electrons participating in the electronic excitations up to a given energy $\hbar\omega$,

$$N_{\text{eff}}(\omega) = \frac{1}{2\pi^2 \mathcal{N}} \int_0^\omega \mathrm{d}\omega' \, \omega' \, \text{Im}\left[\frac{-1}{\epsilon(k = 0, \omega')} \right], \tag{10}$$

tends to the number of electrons filling the orbitals of the gold atom.

We depict in figure 1 the ELF of gold in the optical limit ($k = 0$) and the effective number N_{eff} of target electrons participating in the electronic excitations up to a given energy $\hbar\omega$. The solid curve represents our fitting according to the MELF-GOS method previously described, whereas the symbols are experimental results [21, 22]; the dashed curve represents N_{eff} as a function of the excitation energy $\hbar\omega$. The broad excitation spectrum observed in figure 1 is due to the presence of a large number of inter-band transitions that overlap and interact with collective oscillations [23]. As was mentioned previously, it can be seen that the N-shell does not display the atomic character observed in the K-, L-, and M-shells, given by a sharp edge in the ELF, and hence it cannot be described using GOSs. The parameters we have used to fit the ELF due to outer-shell electrons are given in table 1, whereas the contribution to the ELF from inner-shell electrons belonging to K-, L- and M-shells was evaluated by means of hydrogenic GOS [12]. Figure 1 shows that the ELF smoothly depends on the transferred energy $\hbar\omega$ for the excitations of outer-shell electrons (valence and N-shell electrons), in contrast to the sharp edges observed for the excitations of the electrons belonging to K-, L-, and M-shells.
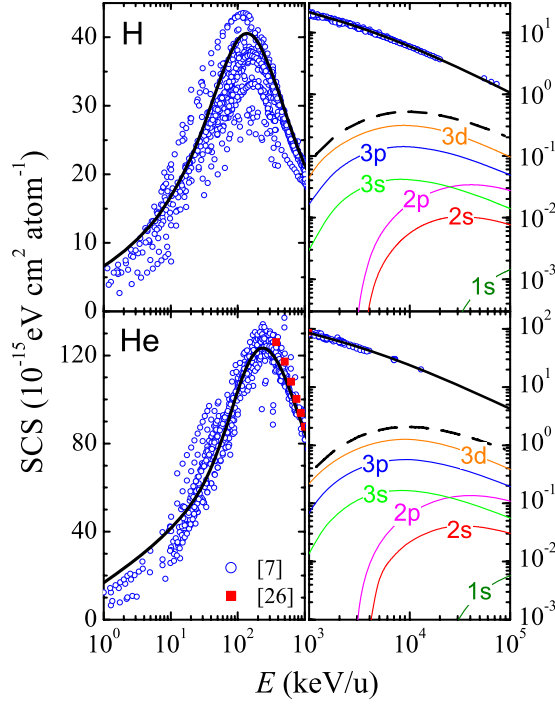
Figure 2. SCS of gold for H and He ions as a function of energy. The thick solid curves represent our calculations, whereas the symbols correspond to the experimental data [7, 26]; thick dashed curves represent the SCS due to inner-shell ionization and the thin solid curves correspond to the SCS associated with each subshell, as indicated in the figure.

As expected N_{eff} increases with the transferred energy $\hbar\omega$, reaching the total number of target electrons $N_{eff} = 79$ for $\hbar\omega \sim 5 \times 10^4$ eV, according to the value of Z_1 for gold.

As an additional check, we evaluate the mean excitation energy of the target, which only depends on the electronic structure of the target [24],

$$\ln I = \frac{\int_0^\infty d\omega\, \omega\, \ln\omega\, \text{Im}\left[-1/\epsilon(k=0, \omega)\right]}{\int_0^\infty d\omega\, \omega\, \text{Im}\left[-1/\epsilon(k=0, \omega)\right]}. \tag{11}$$

We have obtained $I = 754.8$ eV, which is in satisfactory agreement with the currently accepted experimental value of 790 ± 30 eV [25].

We show in figure 2 the stopping cross section (SCS $= S_p/\mathcal{N}$) of Au for H and He ions as a function of their energy. The thick solid curves represent our calculations, whereas the symbols correspond to the experimental data [7, 26]; thick dashed curves represent the SCS due to inner-shell ionization and the thin solid curves correspond to the SCS associated with each subshell, as indicated in the figure. The agreement between our calculations and the available experimental data is quite good in a wide range of projectile energies, but discrepancies between theory and experiment appear at low energies. These discrepancies mainly appear because our calculations are based on the dielectric formalism, which assumes a linear response of the target electrons to the perturbation induced by the projectile. This formalism loses validity as the perturbation grows, i.e. when the projectile has a high charge and low energy. In this situation nonlinear effects, such as the Bloch and Barkas corrections [27], become more significant.
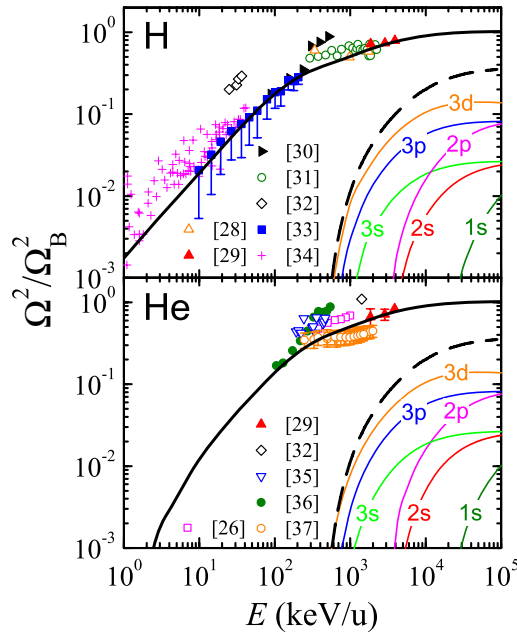
Figure 3. Reduced energy-loss straggling Ω^2/Ω_B^2 of gold for H and He ions as a function of energy. The thick solid curves represent our calculations, whereas the symbols correspond to the experimental data [26, 28–37]; thick dashed curves represent the energy-loss straggling due to inner-shell ionization and the thin solid curves correspond to the energy-loss straggling associated with each subshell, as indicated in the figure.

Our results include the energy loss due to electronic capture and loss processes, although it is worth mentioning that these mechanisms represent a minor contribution to the total SCS, only being appreciable near or before the maximum of the SCS curve. The contribution of the polarization term in equation (2) also represents a minor correction to the SCS. Finally, the SCS due to the target K-, L-, and M-shell ionization is negligible for projectile energies $\lesssim 10^3$ keV/u, i.e. the region comprising the maximum of the SCS, whereas this contribution only starts to be important at high energies and represents ~20% of the total SCS at $\gtrsim 10^5$ keV/u.

We depict in figure 3 the normalized energy-loss straggling Ω^2/Ω_B^2 of Au for H and He ions, with $\Omega_B^2 = 4\pi e^4 \mathcal{N} Z_1^2 Z_2$ being Bohr's energy-loss straggling and Z_2 the target atomic number. The thick solid curves represent our calculations, whereas the symbols and error bars correspond to the experimental data [26, 28–37]; thick dashed curves represent the energy-loss straggling due to inner-shell ionization and the thin solid curves correspond to the energy-loss straggling associated with each subshell, as indicated in the figure. A reasonable agreement between our calculations and the available experimental data is obtained. It is worth mentioning that all the experimental data shown in this figure have corrected the target roughness effect [38, 39], or its contribution has been estimated according to the error bars [33].

The contribution to the energy-loss straggling due to the target K-, L-, and M-shells becomes appreciable for projectile energies $>10^3$ keV/u. In addition, this contribution increases with the projectile energy, being ~35% of the total energy-loss straggling at ~10^4 keV/u, which can be explained according to the ratio $n_{inner}/n = 28/79 \sim 0.35$, where n_{inner} is the number of target inner-shell electrons and n is the number of total target electrons.

The fact that the excitations of the target K-, L-, and M-shells make a more sizable contribution to the energy-loss straggling than to the SCS can be understood considering the dependence on ω^2 in the energy-loss straggling (equation (3)) in comparison with the dependence on ω in the S_p (equation (1)).

In summary, we have calculated the stopping cross section and the energy-loss straggling of Au for swift H and He ions, obtaining quite a good agreement with the available experimental data in a broad energy range. We have paid special attention to an analysis of the contribution of the K-, L-and M-shells to the SCS and Ω^2, finding that it can be neglected for projectiles with energies $\lesssim 10^3$ keV/u. On the contrary, the excitation of the target inner-shell electrons must be considered for projectiles with higher energies, being more important when calculating the energy-loss straggling than the stopping cross section.

Acknowledgments

References

[1] Campbell S A 1996 *The Science and Engineering of Microelectronic Fabrication* (Oxford: Oxford University Press)
[2] Kumakhov M A and Komarov F F 1981 *Energy Loss and Ion Ranges in Solids* (New York: Gordon and Breach)
[3] Turner J 1995 *Atoms, Radiation and Radiation Protection* 2nd edn (New York: Wiley)
[4] Kraft G 2000 *Nucl. Instrum. Methods Phys. Res.* A **454** 1
[5] Leroy C and Rancoita P 2004 *Radiation Interaction in Matter and Detection* (Singapore: World Scientific)
[6] Podgoršak E B 2006 *Radiation Physics for Medical Physicist* (Berlin: Springer)
[7] Paul H, Experimental Stopping Power Compilation. Available from http://www.exphys.uni-linz.ac.at/Stopping/
[8] Abril I, Garcia-Molina R, Denton C D, Pérez-Pérez F J and Arista N R 1998 *Phys. Rev.* A **58** 357
[9] Arista N R and Lifschitz A F 1999 *Phys. Rev.* A **59** 2719
[10] Grande P L and Schiwietz G 2002 *Nucl. Instrum. Methods Phys. Res.* B **195** 55
[11] Sigmund P and Schinner A 2002 *Nucl. Instrum. Methods Phys. Res.* B **195** 64
[12] Heredia-Avalos S, Garcia-Molina R, Fernández-Varea J M and Abril I 2005 *Phys. Rev.* A **72** 052902
[13] Lindhard J 1954 *K. Dan. Vidensk. Selsk. Mat.-Fys. Medd.* **28** (8)
[14] Grande P L and Schiwietz G 2005 *CasP. Convolution Approximation for Swift Particles* version 3.1 (code available at http://www.hmi.de/people/schiwietz/casp.html)
[15] Heredia-Avalos S and Garcia-Molina R 2002 *Nucl. Instrum. Methods Phys. Res.* B **193** 15
[16] Slater J C 1930 *Phys. Rev.* **36** 57
[17] Mermin N D 1970 *Phys. Rev.* B **1** 2362
[18] Planes D J, Garcia-Molina R, Abril I and Arista N R 1996 *J. Electron Spectrosc. Relat. Phenom.* **82** 23
[19] Egerton R F 1989 *Electron Energy-Loss Spectroscopy in the Electron Microscope* (New York: Plenum)
[20] Abril I, Moreno-Marín J C, Fernández-Varea J M, Denton C D, Heredia-Avalos S and Garcia-Molina R 2007 *Nucl. Instrum. Methods Phys. Res.* B **256** 172
[21] Palik E D and Ghosh G (ed) 1999 *The Electronic Handbook of Optical Constants of Solids* (San Diego, CA: Academic)
[22] Henke B L, Gullikson E M and Davis J C 1993 *At. Data Nucl. Data Tables* **54** 181 The ASCII files for the f_1 and f_2 scattering factors of the different elements can be obtained from http://xray.uu.se/hypertext/henke.html
[23] Hagelin-Weaver H A E, Weaver J F, Hoflund G B and Salaita G N 2005 *J. Alloys Compounds* **393** 93
[24] Shiles E, Sasaki T, Inokuti M and Smith D Y 1980 *Phys. Rev.* B **22** 1612
[25] ICRU 1993 *Stopping Powers and Ranges for Protons and Alpha Particles ICRU Report 49* (Bethesda, MD: International Commission on Radiation Units and Measurements)
[26] Amadon S and Lanford W A 2006 *Nucl. Instrum. Methods Phys. Res.* B **249** 34

[27] Sigmund P 2004 *Stopping of Heavy Ions* (Berlin: Springer)
[28] Möller W and Nochen U 1978 *Nucl. Instrum. Methods* **149** 177
[29] Besenbacher F, Andersen J U and Bonderup E 1980 *Nucl. Instrum. Methods* **168** 1
[30] Friedland E and Kotze C P 1981 *Nucl. Instrum. Methods* **191** 490
[31] Alberts H W and Malherbe J B 1983 *Radiatt. Eff.* **69** 231
[32] Yang Q, O'Connor D J and Wang Z 1991 *Nucl. Instrum. Methods Phys. Res.* B **61** 149
[33] Eckardt J C and Lantschner G H 2001 *Nucl. Instrum. Methods Phys. Res.* B **175–177** 93
[34] Andersen H H, Csete A, Ichioka T, Knudsen H, Möller S P and Uggerhöj U I 2002 *Nucl. Instrum. Methods Phys. Res.* B **194** 217
[35] Harris J M and Nicolet M-A 1975 *Phys. Rev.* B **11** 1013
[36] Friedland E and Lombaard J M 1980 *Nucl. Instrum. Methods* **168** 25
[37] Hsu J Y, Yu Y C, Liang J H, Chen K M and Niu H 2004 *Nucl. Instrum. Methods Phys. Res.* B **219/220** 251
[38] Celedon C, Flores M, Häberle P and Valdés J E 2006 *Braz. J. Phys.* **36** 956
[39] Montanari C C, Miraglia J E, Heredia-Avalos S, Garcia-Molina R and Abril I 2007 *Phys. Rev.* A **75** 022903